Journal of Alloys and Compounds 509 (2011) 8137–8143

Contents lists available at ScienceDirect

Journal of Alloys and Compounds

journal homepage: www.elsevier.com/locate/jallcom

First principles study of structural, electronic and magnetic properties of $Mg_{1-x}Mn_xTe$ alloys

N.A. Noor[a], S. Ali[a], W. Tahir[a], A. Shaukat[b], A.H. Reshak[c,d,*]

[a] Department of Physics, University of the Punjab, Quaid-e-Azam Campus, 54590, Lahore, Pakistan
[b] Department of Physics, University of Sargodha, Sargodha 40100, Pakistan
[c] Institute of Physical Biology, South Bohemia University, Nove Hrady 37333, Czech Republic
[d] School of Material Engineering, Malaysia University of Perlis, P.O. Box 77, d/a Pejabat Pos Besar, 01007 Kangar, Perlis, Malaysia

ARTICLE INFO

Article history:
Received 10 March 2011
Received in revised form 22 April 2011
Accepted 25 April 2011
Available online 7 May 2011

Keywords:
$Mg_{1-x}Mn_xTe$ alloys
ab intio calculations
Density functional theory
Electronic band structure
Magnetic properties

ABSTRACT

Density functional FP-LAPW + lo calculations have been performed to study the structural, electronic and magnetic properties of $Mg_{1-x}Mn_xTe$ for compositional parameter $x = 0.25$, 0.50, 0.75 and 1. Our calculations reveal the occurrence of ferromagnetism in these compounds in which the transition-metal atom is ordered in a periodical way thereby interacting directly with the host atoms. Results extracted from electronic band structure and density of states (DOS) of these alloys show the existence of direct energy band gap for both majority- and minority-spin cases, while the total energy calculations confirm the stability of ferromagnetic state as compared to anti-ferromagnetic state. The total magnetic moment for $Mg_{1-x}Mn_xTe$ for each composition is found to be approximately 5 μ_B, which indicates that the addition of Mn content does not affect the hole carrier concentration of the perfect MgTe compound. Moreover, the s–d exchange constant ($N_0\alpha$) and p–d exchange constant ($N_0\beta$) are also calculated which are in accordance with a typical magneto-optical experiment. The estimated spin-exchange splitting energies originated by Mn 3d states energies, i.e. Δ_X(s–d) and Δ_X(p–d), show that the effective potential for minority-spin is more attractive than that of the majority-spin. Also, the p–d hybridization is found to cause the reduction of local magnetic moment of Mn and produce small local magnetic moments on the nonmagnetic Mg and Te sites.

1. Introduction

Due to combined magnetic and semiconducting properties, the dilute magnetic semiconductors (DMSs) have wide range of spintronics applications such as magnetic sensor, optical isolator and non-volatile memory. DMSs are normally III–V, II–VI, II–IV and IV–VI type semiconductors with controlled substitution of constituent atoms by transition metal atoms. The doped transition atoms inject as well as control the spin in the nonmagnetic host atoms [1–3]. The main problem with these materials, from applications point of view, is their low Curie temperature (T_c) which is below room temperature. Because of comparatively high Curie temperature, Mn-doped III–V compounds are most attractive DMSs and their T_c can be enhanced by the improved concentration of Mn. However, the resulting point defects such as Vth group anti-sites and interstitial impurities could compensate hole concentration thereby resulting in the reduction of Curie temperature as per Zener field model [4–6]. DMSs synthesized by the combination of a ferromagnetic material with a semiconductor possess the ability to orient the electron or hole spins even in the absence of external magnetic field. In order to achieve complete spin polarization, however, one has to select a ferromagnetic semiconductor with smaller conductivity than metals, and in this regard II–VI compounds have the advantage to independently control the localized spins and hole concentration [7].

In Mn substituted IIA–VIB compounds, there exists extremely large Zeeman splitting of atomic levels due to strong s, p–d exchange interaction between delocalized band carriers and localized d-shell electrons of Mn^{2+} ions [8], whereas Mg compounds are tetrahedrally bonded with relativity large energy gaps. Since both MgTe and MnTe have quite similar band gaps energies and have a low lattice mismatch between them, one can tune the magnetic properties of ternary compound by varying the ratio of Mg and Mn ions without any significant change in the total band gap energy of the ternary material. Although MgTe and MnTe do not exist in a cubic phase, yet DMS, namely, $Mg_{1-x}Mn_xTe$ has been reported to be grown in a cubic phase for all values of x using MBE [9,10]. To the best of our knowledge no theoretical study, in particular first-

* Corresponding author at: School of Material Engineering, Malaysia University of Perlis, P.O. Box 77, d/a Pejabat Pos Besar, 01007 Kangar, Perlis, Malaysia.
Tel.: +420 777 729 583; fax: +420 386 361 219.
E-mail address: maalidph@yahoo.co.uk (A.H. Reshak).

0925-8388/$ – see front matter © 2011 Elsevier B.V. All rights reserved.
doi:10.1016/j.jallcom.2011.04.133

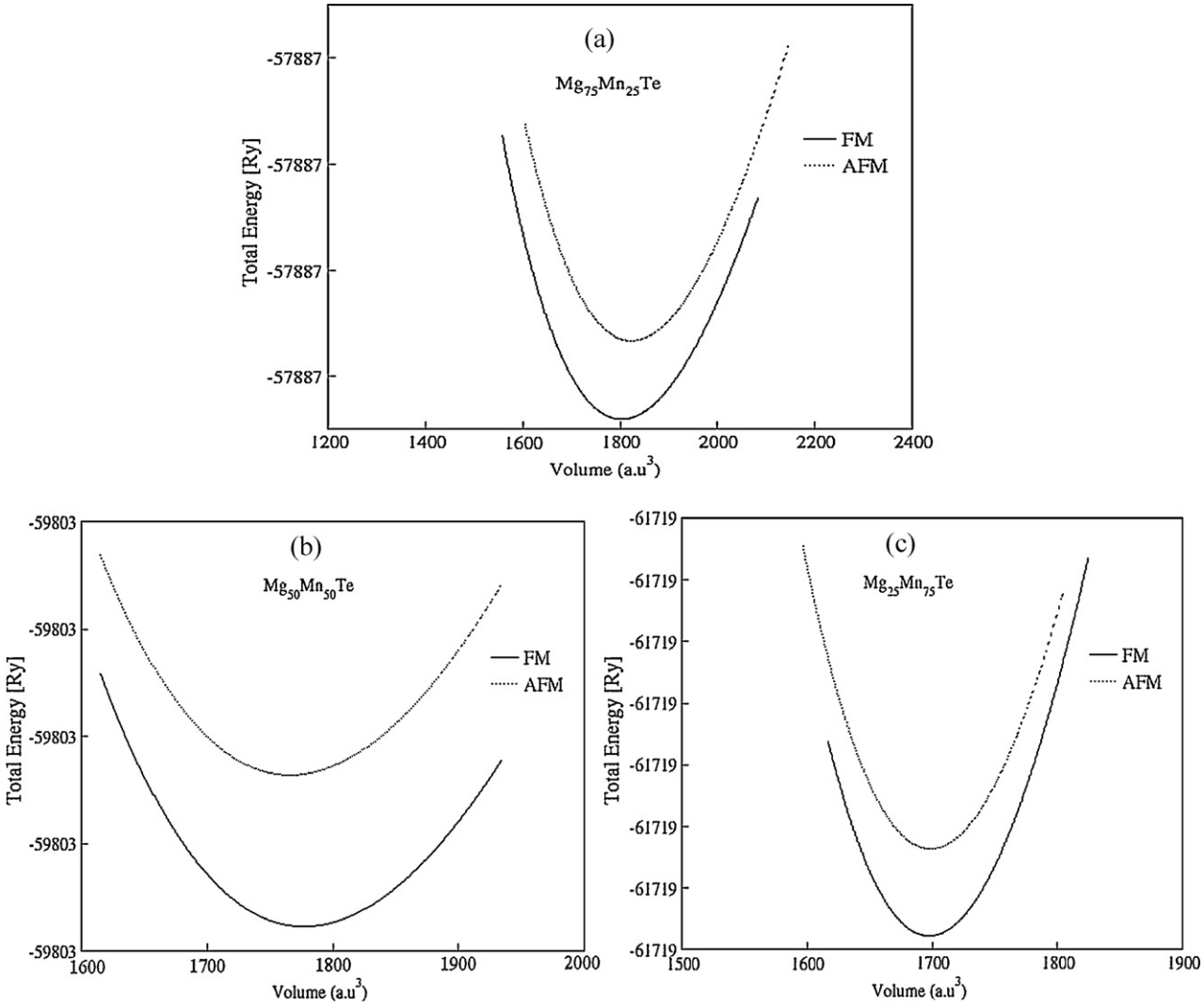

Fig. 1. Calculated total energy versus unit cell volume for $Mg_{1-x}Mn_xTe$, ferromagnetic and anti-ferromagnetic alloys (a) $x = 0.25$, (b) $x = 0.5$, and (c) $x = 0.75$.

principles calculations within density functional theory (DFT) has been undertaken so far on these pseudobinary compounds.

In the present study, we have tried to explore the structural, electronic and magnetic properties of Mn-doped zinc blende MgTe at $x = 0.25$, 0.50, 0.75 and 1.0 using the full potential linearized augmented plane wave plus local orbitals (FP-LAPW + lo) method within the framework of DFT [11,12]. Since Mn-3d and Mg-3s orbitals are difficult to converge so that APW + lo basis set is used inside the atomic sphere, whereas for all other partial waves, we have used LAPW basis set. Furthermore, in the present study, transition-metal atom is ordered in a periodical way in the lattice thereby interacting directly with the host atoms, contrary to the common DMSs in which the diluted limit is at the maximum a few percent, and where, either the distance between the transition-metal atoms is very large (and they can interact only through the conduction electrons) or they form clusters in the semiconductor and different clusters interact between them through the conduction electrons.

2. Details of calculations

Within in the framework of spin-polarized density functional theory, the calculations are performed by WIEN2k code [13] to provide the fundamental understanding of the ground state electronic and magnetic properties of $Mg_{1-x}Mn_xTe$ at $x = 0.25$, 0.50, 0.75 and 1.0. The details for the expansion of Kohn-Sham orbitals by FP-LAPW + lo method are given in the literature [14,15]. In this approach, a muffin-tin (MT) model for the crystal potential is assumed and the electrons are grouped into core electrons, whose charge density is confined to the non-overlapping spheres of radius, R_{MT}, and valence electrons that reside outside the surface of these spheres—the interstitial region (IR). Inside each MT sphere, the basis set is splitted into core and valence subsets. The calculations for the core states are carried out within the spherical part of the potential only. However, the valence states calculations are carried out within a potential expanded into spherical harmonics. The exchange and correlation potentials were calculated by generalized gradient approximation (GGA) proposed by Wu–Cohen [16], which is advantageous for magnetic system. Neglecting the spin orbital coupling, the scalar style relativistic effect is taken into account.

Taking zinc blende standard unit cell of $1 \times 1 \times 1$, we obtained the structures of $Mg_{1-x}Mn_xTe$ ($x = 0.25$, 0.50 and 0.75) by replacing the Mg atoms with Mn to get the alloys with 25%, 50% and 75% concentration, respectively. For alloys, randomness can be reproduced for the first few shells around a given site, with the help of 'special quasirandom structures' (SQSs) approach [17]. The concept of SQSs, which are specially designed small-unit-cell periodic structures with only a few (2–16) atoms per unit cell, was proposed by Zunger et al. [17] to study the properties of random substitutional alloys,

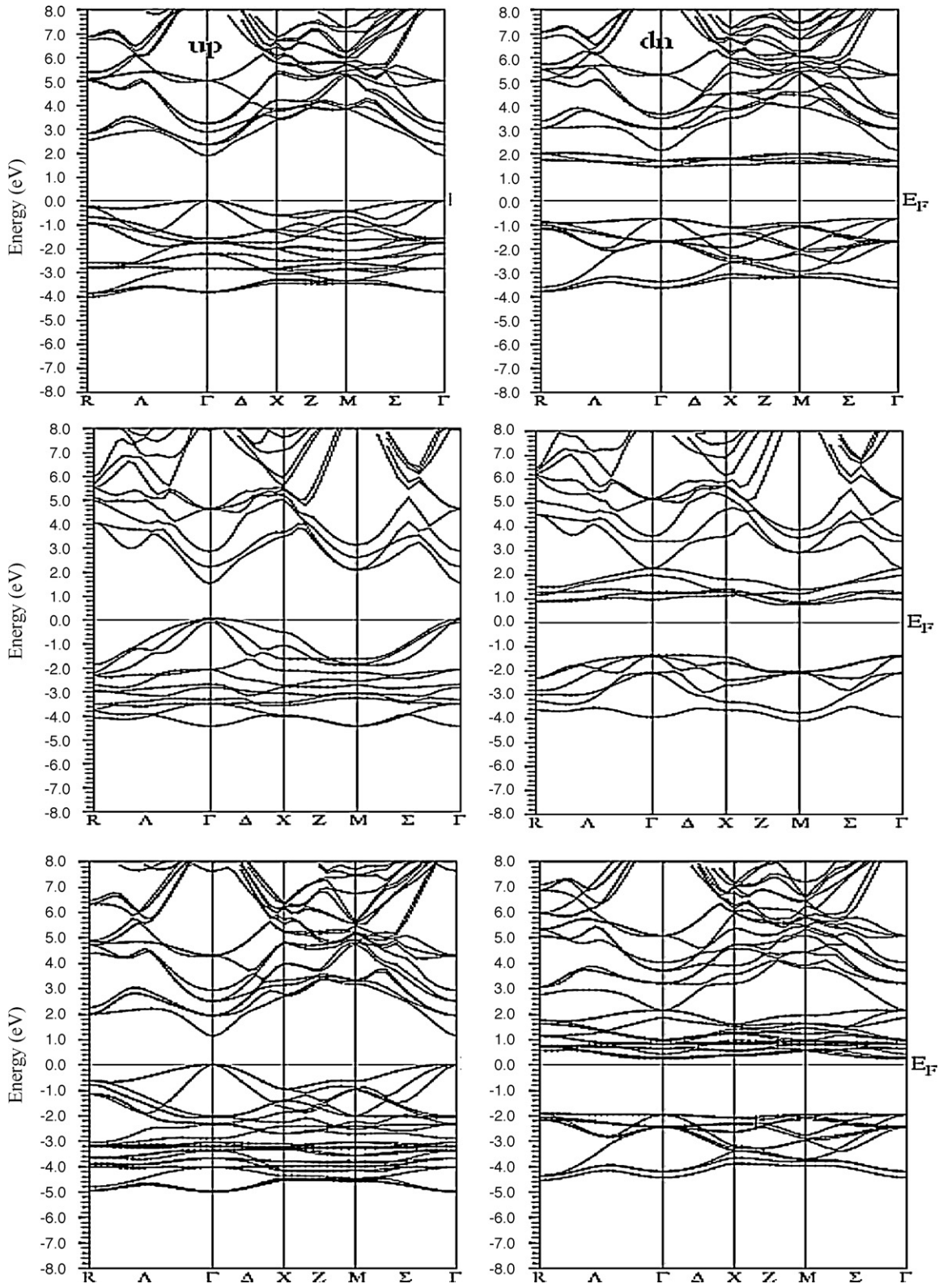

Fig. 2. Calculated band structure of $Mg_{0.75}Mn_{0.25}Te$, $Mg_{0.50}Mn_{0.50}Te$ and $Mg_{0.25}Mn_{0.75}Te$ along the selected high symmetry directions. The left panels are the majority-spin bands and the right panels the minority-spin.

as SQSs reproduce the most relevant, near-neighbor pair and multisite correlation functions of theses alloys. Since first-principles calculations based on DFT rely on the construction of cells with periodic boundary conditions, these calculations are relatively straight-forward, as long as the material is a perfectly ordered structure. However, for random substitutional alloys these calculations become complicated, and one requires large supercells, which are computationally constrained by the number of atoms that one can treat. In SQSs approach, one is dealing with a distribution of distinct environment, the average of which corresponds to the

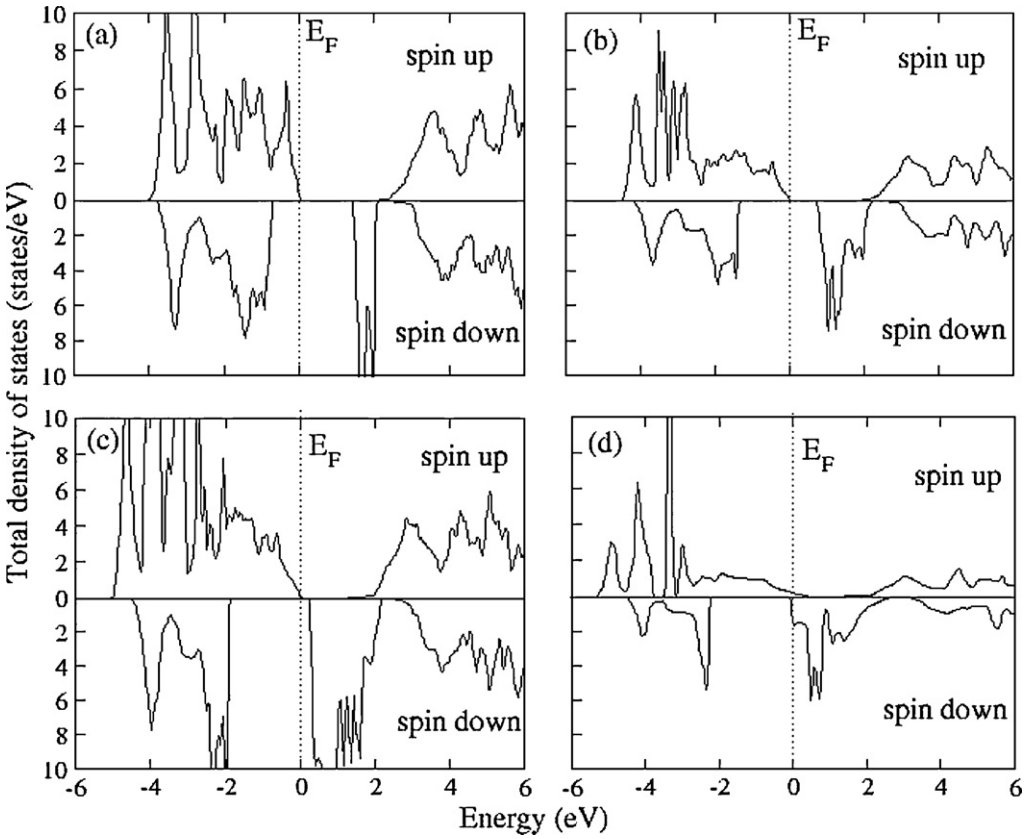

Fig. 3. Spin-dependent TDOS of $Mg_{1-x}Mn_xTe$ for (a) $x = 0.25$, (b) $x = 0.5$, (c) $x = 0.75$ and (d) $x = 1.0$.

random alloy [18], thereby reducing the periodicity errors which occur when we describe random alloys with periodic structures. In the present study, total energy calculations (for both ferromagnetic and antiferromagnetic cases) have been performed by using SQSs for the three compositions $x = 0.25$, 0.50 and 0.75, and to study the electronic and magnetic properties of the alloys. We have used 2.47 Bohr as muffin-tin value for transition-metal Mn and 2.33, 2.19 Bohr for Mg and Te, respectively. The maximum value of angular momentum for the wave function expansion inside the sphere ($l_{max} = 10$) and density plane cut-off ($R_{MT} \times K_{max} = 8$) are used in our calculations. A modified tetrahedron method is applied for BZ integrations by taking 2000 **k**-points for ferromagnetism calculations and 1000 **k**-points for anti-ferromagnetic calculations. The self-consistent calculations are considered to converge only when the calculated total energy converges is less than 0.0001 Ry.

3. Results and discussion

3.1. Structural properties

Since optimization is vital to reflect truly the ferromagnetism of the doping system, structural properties of $Mg_{1-x}Mn_xTe$ ($x = 0.25$, 0.50, 0.75 and 1.0) are studied using structural optimization by minimizing the total energy as a function of the unit cell volume with the help of Murnagnan's equation of state [19], and the values of calculated structural parameters such as equilibrium lattice constants and bulk moduli are listed in Table 1. Also, the calculated total energy verses unit cell volume of $Mg_{1-x}Mn_xTe$ at $x = 0.25$, 0.50 and 0.75 for both ferromagnetic (FM) and anti-ferromagnetic (AFM) are shown in Fig. 1. For both ferromagnetic (FM) and anti-ferromagnetic (AFM) phases, the ground state of $Mg_{1-x}Mn_xTe$ alloy was found by performing self-consistent calculations. Parallel spin directions were found for the two Mn cations in the FM state; however in AFM state the two magnetic cations have anti-parallel spins. Results show that for these alloys the total energy difference ($\Delta E = E_{AFM} - E_{FM}$) between AFM and FM states are positive, i.e. ferromagnetic states are more stable than anti-ferromagnetic states and the total energy differences between the said states of $Mg_{1-x}Mn_xTe$ per Mn atom are 0.2013, 0.2952, 0.4463 and 0.0012 eV for $x = 0.25$, 0.50, 0.75 and 1.0, respectively.

3.2. Electronic band structure, DOS, charge densities

Spin-polarized band structures of $Mg_{1-x}Mn_xTe$ ($x = 0.25$, 0.50 and 0.75) for spin-up and spin-down alignments are shown in Fig. 2 along the high symmetry directions in the first Brillouin zone. Both

Table 1
Calculated zincblende phase values of equilibrium lattice constants a (Å), bulk modulus B (GPa), the total magnetic moments per Mn (M_{tot} in μ_B) and local magnetic moment of Mn Mg and Te in $Mg_{1-x}Mn_xTe$.

Compound	a (Å)	B (GPa)	M_{tot}	M_{Mn}	M_{Mg}	M_{Te}
$Mg_{0.75}Mn_{0.25}Te$	6.43	36.17	5.000	4.370	0.01826	0.0229
$Mg_{0.50}Mn_{0.50}Te$	6.40	38.85	5.000	4.394	0.038	0.0431
$Mg_{0.25}Mn_{0.75}Te$	6.33	42.13	5.000	4.421	0.059	0.0632
MnTe	6.25, 6.34[a]	45.01	5.000	4.400	–	0.0666

[a] Ref. [24].

Table 2
Calculated ferromagnetic (FM) energy band gap E_g (eV) and conduction and valence band-edge spin-splitting ΔE_c and ΔE_v and exchange constants of $Mg_{1-x}Mn_xTe$ for (a) $x = 0.25$, (b) $x = 0.5$, (c) $x = 0.75$ and (d) $x = 1.0$.

Compounds	E_g (eV)	ΔE_c	ΔE_v	$N_0\alpha$	$N_0\beta$
$Mg_{0.75}Mn_{0.25}Te$ (FM)	1.31	0.60	−0.72	1.08	−1.318
$Mg_{0.50}Mn_{0.50}Te$ (FM)	0.60	1.04	−1.32	0.95	−1.201
$Mg_{0.25}Mn_{0.75}Te$ (FM)	0.19	1.33	−1.91	0.82	−1.150
MnTe (FM)	0.00	1.69	−2.21	0.76	−1.005
MnTe (AFM)	1.20, 1.28[a]	0.82	−2.30	0.37, 0.34[a]	−1.045, −1.10[a]
$Mg_{0.67}Mn_{0.33}Te$				0.20[b]	−0.50[b]

[a] Ref. [20].
[b] Ref. [25].

spin-up and spin-down band structures show that the top of the valence band and bottom of the conduction band are located at Γ point. This indicates that a direct energy gap at high symmetry point is associated with spin-up as well as spin-down band structure. Calculated values of the energy band gap are displayed Table 2, where we have indicated both band-gap values of MnTe corresponding to ferromagnetic and antiferromagnetic phases. Ferromagnetic zinc blende MnTe appears to be metallic, as one can see in Table 2, while antiferromagnetic phase turns out to be a semiconductor. Our results are in conformity with an earlier electronic structure study undertaken by Fleszar et al. [20], based on local spin-density approximation (LSDA) and the GW approach. The calculated total and partial density of states of $Mg_{1-x}Mn_xTe$ ($x = 0.25$, 0.50, 0.75 and 1.0), which are presented in Figs. 3 and 4, show the involvement of 3d states of Mn ions with small contribution of 3p of Mg and 5p states of Te ions in energy range −4.12 to −0.15 eV, while the upper valence band for spin-up states is quite different from that spin-down states. From Fig. 3, which is drawn for alloys with doping concentration at $x = 0.25$, the occupied Mn-3d bands with spin-up configuration are observed that are centered at

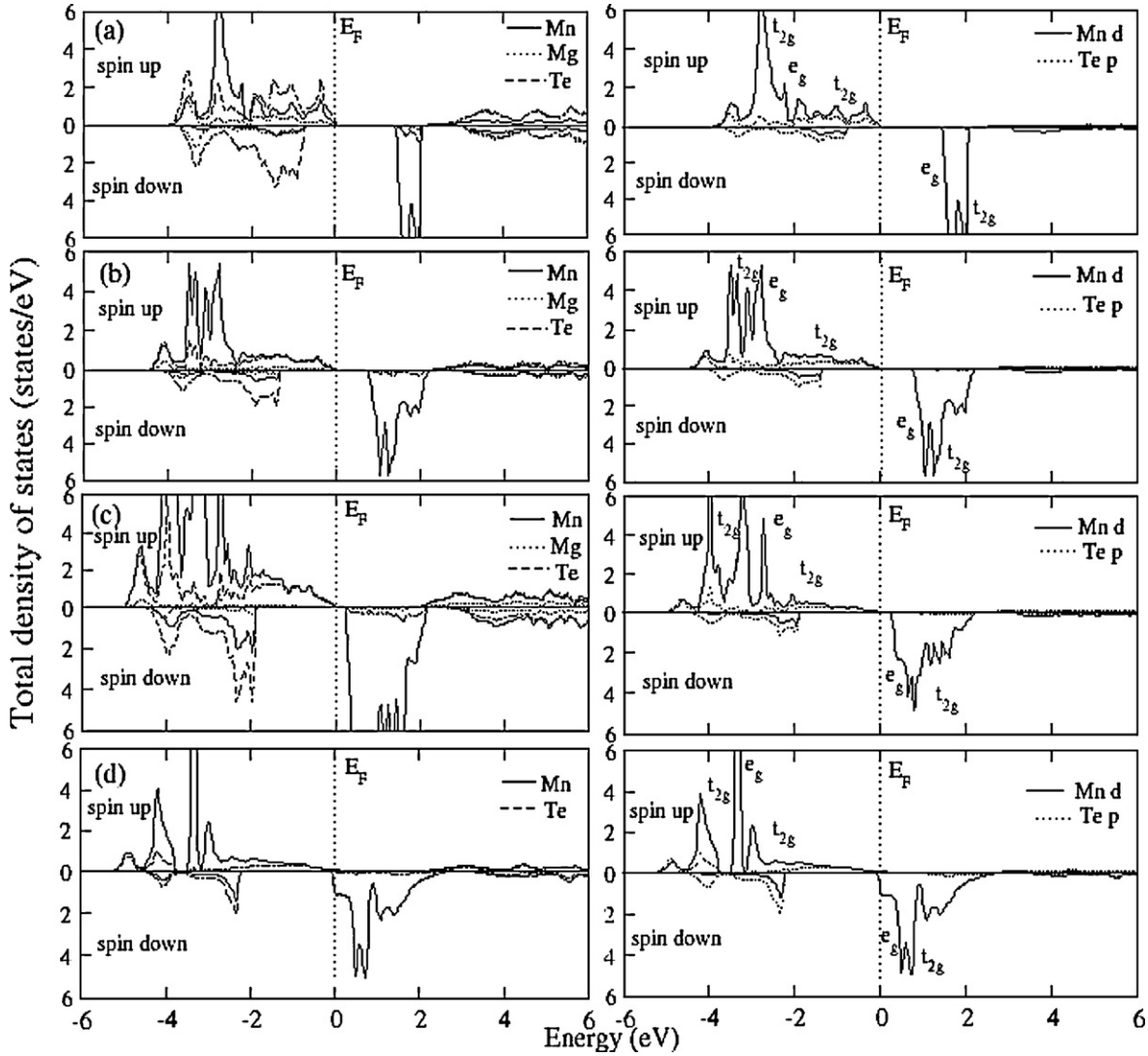

Fig. 4. Spin-dependent PDOS projected in Mn (solid line), Mg (dotted line) and Te (dashed line) at (a) $x = 0.25$, (b) $x = 0.5$, (c) $x = 0.75$ and (d) $x = 1.0$ atoms of $Mg_{1-x}Mn_xTe$ (left side). Right side is the DOS of Mn d e_g and d t_{2g} states.

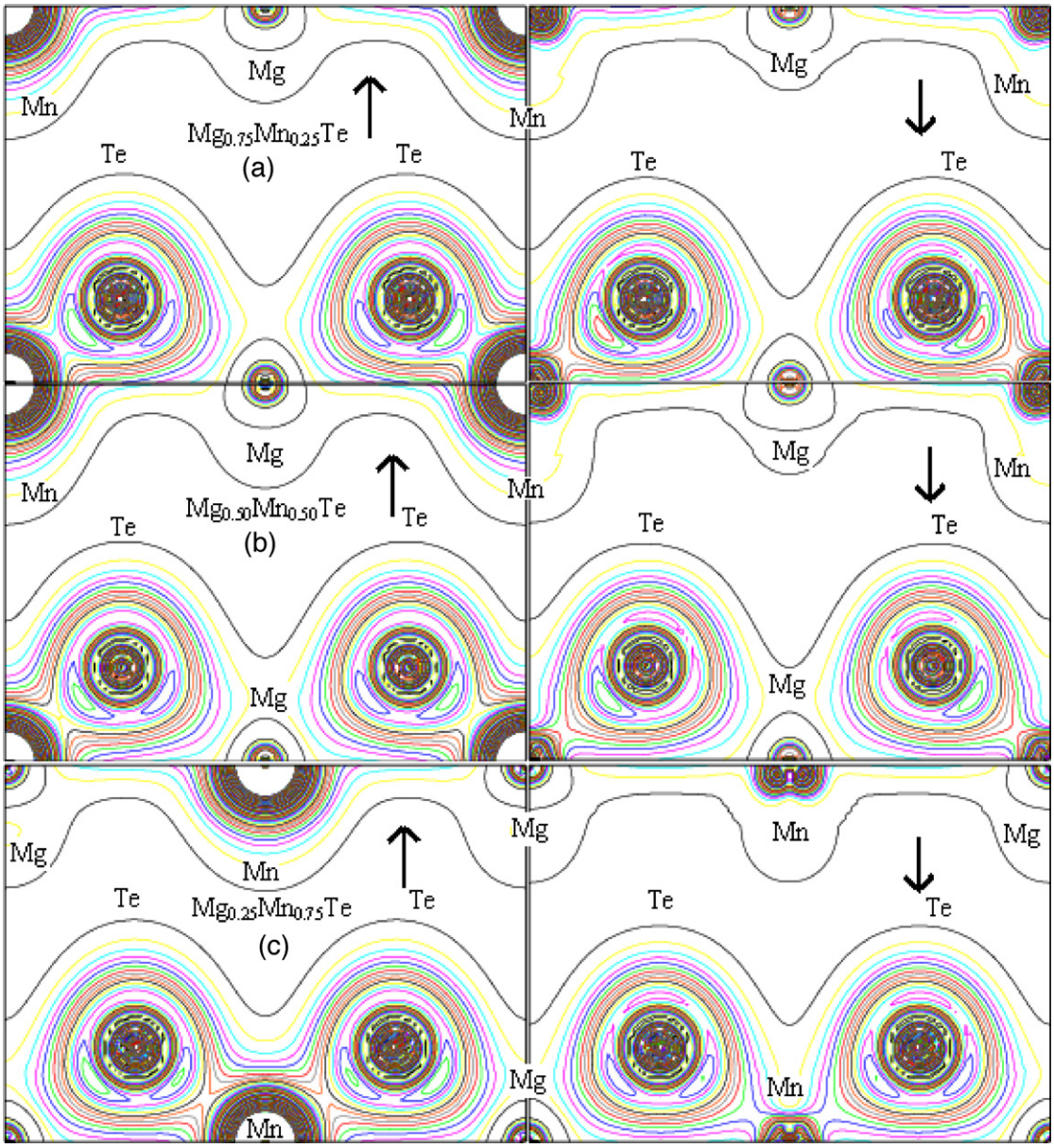

Fig. 5. Calculated spin-dependent charge density contours projected (1 1 0) plane for $Mg_{1-x}Mn_xTe$ at $x = 0.25$, 0.50 and 0.75.

$E_v^{\uparrow} = -2.82$ eV, while the spin-down Mn 3d bands are empty and centered at $E_v^{\downarrow} = +1.67$ eV. Here $E_v^{\uparrow}$ and $E_v^{\downarrow}$ are the valence band maxima for spin-up and spin-down, respectively Similarly, for doping concentrations at $x = 0.50$, 0.75 and 1.0, the occupied Mn 3d bands with spin-up configuration are observed that are centered at −3.07 eV, −3.25 eV and −3.31 eV, while the spin-down Mn 3d bands are empty and centered at +1.24 eV, +0.89 eV and +0.49 eV, respectively.

The separation between the spin-up and spin-down peaks is known as spin exchange splitting which is represented by $\Delta_X(\mathrm{d}) = E(C_{\mathrm{d}}^{\downarrow}) - E(C_{\mathrm{d}}^{\uparrow})$, and its values for Mn 3d states of $Mg_{1-x}Mn_xTe$ is found to be +4.75 eV, +4.98 eV, +5.25 eV and 5.63 eV at $x = 0.25$, 0.50, 0.75 and 1.0, respectively. The values of crystal field splitting, defined as $\Delta E_{\mathrm{crystal}} = E_{t_{2g}} - E_{e_g}$ for these concentration are 1.08 eV, 0.82 eV, 0.74 eV and 0.62 eV, respectively. These results show that for each concentration, the spin exchange splitting is larger than the crystal field splitting. To explain the nature of attraction, p–d exchange splitting parameter $\Delta_X(\mathrm{pd}) = E_v^{\downarrow} - E_v^{\uparrow}$ is calculated and its values are found to be −0.72 eV, −1.32 eV, −1.91 eV and −2.21 eV for $x = 0.25$, 0.50, 0.75 and 1.0, respectively. These values indicate that the effective potential for the minority-spin is more attractive than that for the majority-spin [21].

Our calculations of the charge spin densities for $Mg_{1-x}Mn_xTe$ ($x = 0.25$, 0.50, 0.75) alloys in the (1 1 0) plane elucidates the nature of the bonding in different phases as shown in Fig. 5. For the concentration $x = 0.25$, the contour plot shows partial ionic and covalent bonding, indicating a strong covalent MnTe bond and ionic character of MgTe bond. The nature of bonds remains same for both spin-up and spin-down cases. However, as the Mn concentration is increased form 0.25 to 0.75, not only the Mn–Te bond becomes stronger, some polarization of Mg–Te bond is also observed, making it a little more covalent. Relatively more ionic behavior of Mn–Te bond than that of Mg–Te bond can be attributed to the increase in electronegativity difference between the two atoms which in turn increases the displacement of bonding charge. Similarly, weak covalent bonding is observed in both Mg–Te bond and Mn–Te bond at $x = 0.50$ and covalent bond is stronger at Mg–Te bond than the Mg–Te bond.

3.3. Exchange coupling, magnetic moments

To study the magnetic as well as thermodynamic properties, evaluation of exchange constants $N_0\alpha$ and $N_0\beta$ is required. In order to take into the account the influence of valence and conduction bands in the process of exchange and splitting, it is convenient to parameterize the spin-splitting of conduction and valence bands. This interpretation is in accordance with mean field theory based on the Hamiltonian given by the following equation [22,23]:

$$H = -N_0\beta s \cdot S,$$

where N_0 is the concentration of cations, β is the p–d exchange integral and s and S are the hole spin and the Mn spin, respectively. Similar argument can also be applied for spin splitting of the conduction band, based on the same Hamiltonian with $N_0\alpha$ exchange constant. The exchange constants can be calculated directly from the valence and conduction band-edge spin splitting $\Delta E_c = E_c^{\downarrow} - E_c^{\uparrow}$ and $\Delta E_v = E_v^{\downarrow} - E_v^{\uparrow}$ using the following equations:

$$N_0\alpha = \frac{\Delta E_c}{x\langle S\rangle}, \quad N_0\beta = \frac{\Delta E_v}{x\langle S\rangle}$$

Our calculated values of ΔE_c, ΔE_v, $N_0\alpha$ and $N_0\beta$ are presented in Table 2. The above findings confirm the ferromagnetic of nature of p–d coupling between the conduction band of MgTe and the Mn impurity, which in turn labels the magnetic character to these materials.

The calculated values of the total and local magnetic moments for DMSs $Mg_{1-x}Mn_xTe$ at $x = 0.25$, 0.50, 0.75 and 1.0 within the muffin-tin spheres are listed in Table 1. For $Mg_{1-x}Mn_xTe$ at $x = 0.25$, 0.50, 0.75 and 1.0, the total magnetic moment of 3d electrons within the sphere is found to be 5.00023, 5.00026, 5.00028 and 4.91488 μ_B, respectively. The presence of permanent local magnetic moments can be attributed to the partially filled Mn 3d states. The magnetic ions and the electrons or holes near the band edges interact with each other via long oscillatory exchange interactions. In return, these interactions endow special properties to DMSs. Here, we also report the observation of the reduction of local Mn moments due to p–d hybridization along with induction of local magnetic moments in the neighboring nonmagnetic (Mg, Te) atoms.

4. Conclusion

In this work, we have applied the successful (FP-LAPW + lo) method which enables the direct evaluation of the spin-based electronic and magnetic properties of the DMSs $Mg_{1-x}Mn_xTe$ at $x = 0.25$, 0.50, 0.75 and 1, in the ferromagnetic phase. The calculations are performed within the framework of spin-polarized density functional theory with generalized gradient approximation. The hybridization of valence 3d electrons in Mn ions elucidates the presence of well defined spin-up and spin-down band structures in all compositions. The results based on partial densities of states allow us to find both the exchange splitting Δ_X(d) and Δ_X(pd) and the crystal field splitting originated by Mn 3d states. Our results give unambiguous evidence for effective potential, clarifying its attractiveness for minority-spin than that for majority-spin. Another important result regarding to total and local magnetic moments is that the addition of Mn ions introduces no hole carrier to the host MgTe crystal. The value of total magnetic moment has been calculated to be 5 μ_B. It is found that the unfilled Mn 3d states, together with p–d hybridization results in significant decrease in the local magnetic moment at the Mn site from its free-space value, leading to the generation of a small local magnetic moment at Mg and Te sites.

Acknowledgements

For the author Ali H. Reshak his work was supported from the institutional research concept of the Institute of Physical Biology, UFB (No. MSM6007665808), the program RDI of the Czech Republic, the project CENAKVA (No. CZ.1.05/2.1.00/01.0024), the grant No. 152/2010/Z of the Grant Agency of the University of South Bohemia. School of Material Engineering, Malaysia University of Perlis, P.O. Box 77, d/a Pejabat Pos Besar, 01007 Kangar, Perlis, Malaysia.

References

[1] K. Ganesan, S. Mariyappan, H.L. Bhat, Solid State Commun. 143 (2007) 272.
[2] Y. Kimishima, M. Uehara, K. Irie, S. Ishihara, T. Yamaguchi, M. Saitoh, K. Kimoto, Y. Matsui, J. Magn. Magn. Mater. 320 (2008) 674.
[3] S.J. Pearton, C.R. Abernathy, G.T. Thaler, R. Frazier, F. Ren, A.F. Hebard, Y.D. Park, D.P. Norton, W. Tang, M. Stavola, J.M. Zavada, R.G. Wilson, Physica B 340 (2003) 39.
[4] H. Raebiger, T. Hynninen, A. Ayuela, J. von Boehm, Physica B 376–377 (2006) 634.
[5] C. Zener, Phys. Rev. 83 (1951) p299.
[6] Y. Guo, M. Chen, Z. Guo, X. Yan, Phys. Lett. A 372 (2008) 2688.
[7] L. Hansena, D. Ferrand, G. Richter, M. Thierley, V. Hock, N. Schwarz, G. Reuscher, G. Schmidt, L.W. Molenkamp, A. Waag, Appl. Phys. Lett. 79 (2001) 3125.
[8] J.K. Furdyna, J. Appl. Phys. 64 (1988) p4.
[9] E. Janik, E. Dynowska, J.B. Misiuk, T. Wojtowicz, G. Karczewski, J. Kossut, A.S. Wojcik, A. Twardowski, W. Mac, K. Ando, J. Cryst. Growth 184/185 (1998) 976.
[10] S. Mackowski, E. Janik, F. Kyrychenko, J. Kossut, Thin Solid Films 367 (2007) 223.
[11] P. Hohenberg, W. Khon, Phys. Rev. 136 (1964) B864.
[12] W. Kohn, J.L. Sham, Phys. Rev. 140 (1965) A1133.
[13] P. Blaha, K. Schwarz, G.K.H. Madsen, D. Kvasnicka, J. Luitz, WIEN2K, an augmented plane wave + local orbitals program for calculating crystal properties, KarlheinzSchwarz, Techn. Universität, Vienna, Austria, 2001.
[14] E. Sjöstedt, L. Nordstörm, D.J. Singh, Solid State Commun. 114 (2000) 15.
[15] K. Schwarz, P. Blaha, G.K.H. Madsen, Comput. Phys. Commun. 147 (2002) 71.
[16] Z. Wu, R.E. Cohen, Phys. Rev. B 73 (2006) 235116.
[17] A. Zunger, S.H. Wei, L.G. Ferreira, E. Bernard, Phys. Rev. Lett. 65 (1990) 353.
[18] C. Jiang, C. Wolverton, J. Sofo, L.-Q. Chen, Z.-K. Liu, Phys. Rev. B 69 (2004) 214202.
[19] F.D. Murnaghan, Proc. Natl. Acad. Sci. USA 30 (1944) 244.
[20] A. Fleszar, M. Potthoff, W. Hanke, Phys. Status Solidi (c) 4 (2007) 3270.
[21] V.L. Morozzi, J.F. Janak, A.R. Williams, Calculated Electronic Properties Metals, Pergamon, New York, 1978.
[22] G.A. Gaj, R. Planel, G. Fishman, Solid State Commun. 29 (1979) 435.
[23] S. Sanvito, P. Ordejon, N.A. Hill, Phys. Rev. B 63 (2001) 165206.
[24] H. Anno, T. Koyanagi, K. Matsubara, J. Cryst. Growth 117 (1992) 816.
[25] I. Kuryliszyn, A.S. Wojcik, A. Twardowski, E. Janik, E. Dynowska, J.B. Misiuk, Solid State Commun. 122 (2002) 213.